

# Generative Photomontage

Sean J. Liu<sup>1</sup>    Nupur Kumari<sup>1</sup>    Ariel Shamir<sup>2</sup>    Jun-Yan Zhu<sup>1</sup>

<sup>1</sup>Carnegie Mellon University    <sup>2</sup>Reichman University

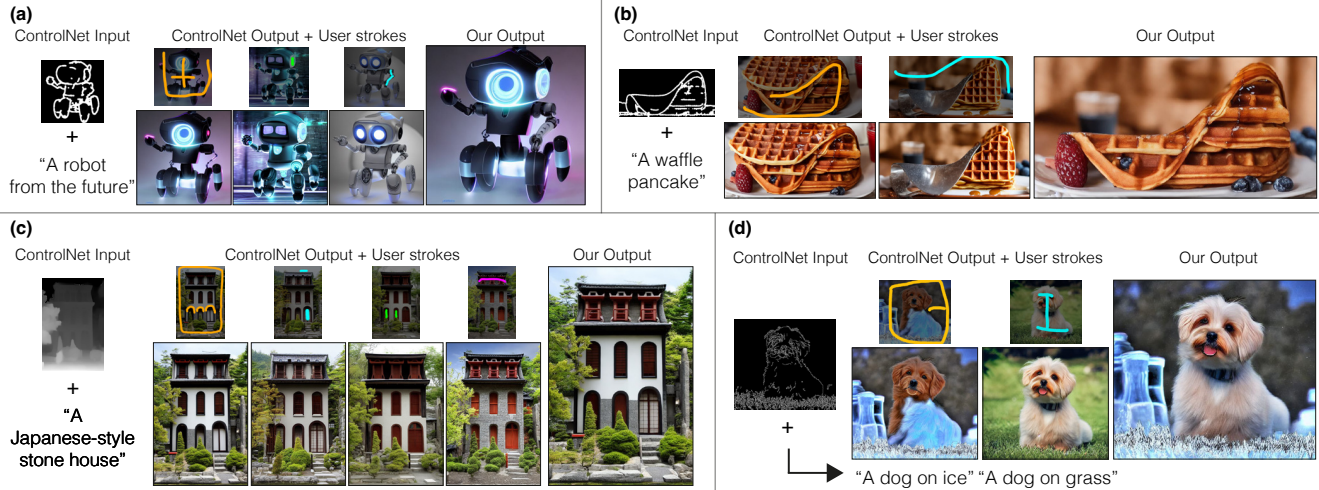


Figure 1. We introduce Generative Photomontage, a framework that allows users to create their desired image by *compositing* multiple generated images. Given a stack of ControlNet-generated images using the same input condition and different seeds, users select desired regions from different images within the stack. Our method takes in the user strokes, solves for a segmentation across the stack using diffusion features, and then composites them using a new feature-space blending method. Our method offers users fine-grained control over the final image and enables various applications, such as generating unseen appearance combinations (a, c), correcting shapes and removing artifacts (b, d).

## Abstract

Text-to-image models are powerful tools for image creation. However, the generation process is akin to a dice roll and makes it difficult to achieve a single image that captures everything a user wants. In this paper, we propose a framework for creating the desired image by compositing it from various parts of generated images, in essence forming a Generative Photomontage. Given a stack of images generated by ControlNet using the same input condition and different seeds, we let users select desired parts from the generated results using a brush stroke interface. We introduce a novel technique that takes in the user’s brush strokes, segments the generated images using a graph-based optimization in diffusion feature space, and then composites the segmented regions via a new feature-space blending method. Our method faithfully preserves the user-selected regions while compositing them harmoniously. We demonstrate that our flexible framework can be used for many applications,

including generating new appearance combinations, fixing incorrect shapes and artifacts, and improving prompt alignment. We show compelling results for each application and demonstrate that our method outperforms existing image blending methods and various baselines.

## 1. Introduction

Text-to-image models [61, 84] can generate visually compelling images from simple input conditions, such as text prompts and sketches, making them a powerful tool for image synthesis and creative exploration.

However, these models may not achieve exactly what a user envisions, due to the ambiguity in mapping from lower-dimensional input space (e.g., text, sketch) to high-dimensional pixel space. For example, the prompt “a robot from the future” can map to any sample in a large space of robot images, that is usually sampled using different random seeds in the diffusion process. From the user’s perspective,

this procedure is akin to a dice roll. In particular, it is often challenging to achieve a *single* image that includes everything the user wants: the user may like one part of the robot from one result and another part in a different result. They may also like the background in yet a third result.

Many works add various conditions to text-to-image models for greater user control [52, 84], such as edges and depth maps. While these approaches restrict the output space to better match the additional user inputs, the process is still akin to a dice roll (albeit with a constrained die). For example, using the same edge map and text prompt, ControlNet [84] can generate a range of outputs that differ in lighting, appearance, and backgrounds. Some results might contain desirable visual elements, while others could contain artifacts or fail to adhere closely to the input conditions. While one can create numerous variations using different random seeds (i.e., re-roll the dice), such a trial-and-error process offers limited user control and makes it challenging to achieve a completely satisfactory result.

In this paper, we propose a different approach – we suggest the possibility of synthesizing the desired image by *compositing* it from different parts of generated images. We refer to the final result as a *Generative Photomontage*, inspired by the seminal work of Interactive Digital Photomontage [1]. In our approach, users can first generate many results (roll the dice first) and then choose exactly what they want (composite across the dice rolls), which gives users fine-grained control over the final output and significantly increases the likelihood of achieving their desired result. Our key idea is to treat generated images as intermediate outputs, let users select desired parts from the generated results, and then composite the user-selected regions to form the final image.

Our framework begins with a *stack* of images from ControlNet, generated by using the same text prompt and control inputs, and lets users choose parts they like from different images via simple brush strokes. Our key insight is that these images share common spatial structures from the same input condition, which can be leveraged for composition. We propose a novel technique that takes in the user’s brush strokes, segments the image parts in diffusion feature space, and then composites these parts during a final denoising process. Specifically, given users’ sparse scribbles, we formulate a multi-label graph-based optimization in diffusion feature space, grouping regions with similar diffusion features while satisfying user inputs. We then introduce a new feature injection and mixing method to composite the segmented regions. Our method accurately preserves the user-selected regions while harmoniously blending them together.

The advantages of using our approach are two-fold. First is the user interaction. Our approach strikes a balance between exploration and control: by treating the model’s generated images as intermediate outputs and allowing users to select and composite across them, users can take advantage

of the model’s generative capabilities and use it as an exploration tool, while also retaining fine-grained control over the final result. This is especially helpful in cases where users may not know what they want until they see it. Second is the ability to correct undesired artifacts in resulting images. With our method, users can replace undesired regions with more visually appealing regions from other images and build towards their desired result. Compared to the trial-and-error process, where users “re-roll the dice” in hopes of getting a satisfactory image, our approach combinatorially improves the chances of success: users can combine a few images, each one containing a good region.

We show visually compelling results on various applications and user workflows, including creating new appearance combinations, correcting shape misalignment, reducing artifacts, and improving prompt alignment. Our method outperforms existing pixel-space blending methods in preserving the realism and fidelity of local regions. Our code, data, and additional results are available on our [webpage](#).

## 2. Related Work

**Text-to-image generative models** aim to learn the real image distribution conditioned on textual inputs [53, 74, 89]. In recent years, we have seen rapid progress with works on different training objectives, such as diffusion [32, 38, 39, 70, 71], GANs [37, 65, 66], and autoregressive models [16, 82], as well as new architectures [20, 21, 58, 61]. However, these models may still fall short of generating what the user wants in one go and often fail to follow all instructions in the text prompt, despite recent efforts [17, 23, 49]. In this work, we aim to bridge this gap by allowing users to compose desirable regions from multiple generated images.

**Image editing.** Text-to-image diffusion models have enabled various editing tasks given reference images and text-instructions [26, 31, 34, 51, 80, 81, 87]. This is usually achieved through fine-tuning the model [12, 40] or modifying the denoising process of the diffusion model [2, 14, 30, 35, 51, 55, 76]. These methods often focus on the attention mechanism in the text-to-image model, which is crucial for determining the structure and text alignment of generated images [30, 57]. While we take inspiration from these works, our tasks and methods are different. Notably, MasaCtrl [14], Cross-Image Attention [2], and StyleAligned [31] focus on high-level style transfer, where local appearances are expected to change. We focus on blending a multi-image stack and preserving local appearances for greater user control. In contrast to their approaches, which perform full image feature injection, our method solves for and injects a *composite* of features from multiple images, computed from a graph-cut optimization. We show that our proposed technique performs better for this new task.

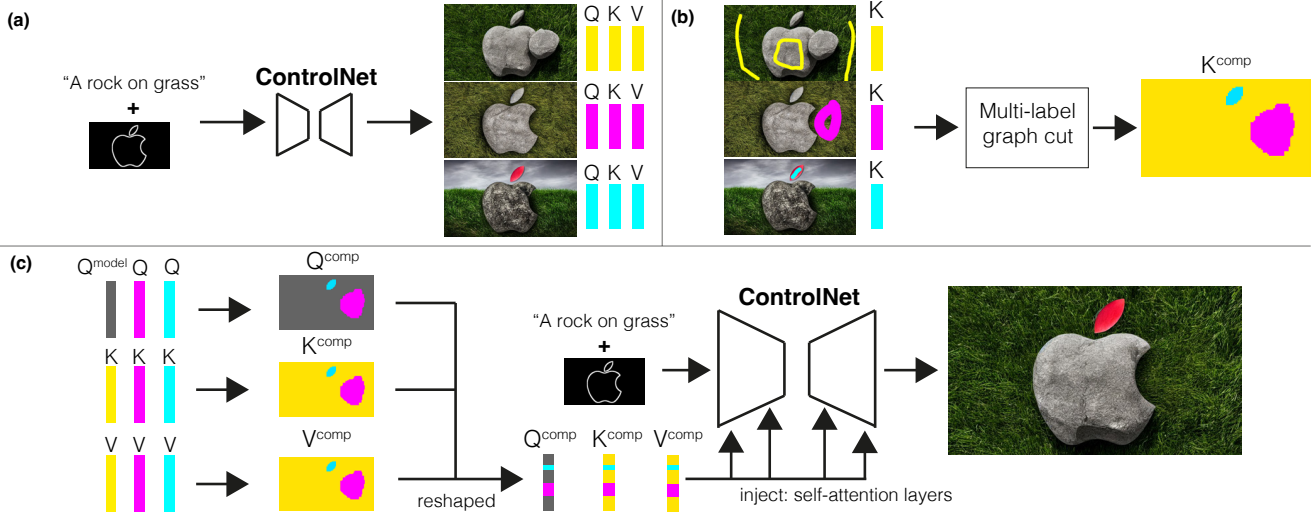


Figure 2. **Overview.** (a) ControlNet-generated images using the same prompt and sketch with different seeds. (b) Upon inspecting the stack, the user wishes to remove the extra rock from the first image and add in the red leaf from the third image. The user draws strokes to select desired regions from each image. Our method finds a segmentation across the stack by performing multi-label graph cut in diffusion feature space ( $K$  features). (c) The graph-cut result is then used to form composite  $Q$ ,  $K$ ,  $V$  features, which are then injected into the self-attention layers. The final result is a harmonious composite of the user-selected regions.

**Controllable image generation.** Improving controllability and adherence to text instructions is critical for using these models as a collaborative tool. As a result, many recent works increase user control in the form of input conditions, such as sketch, depth map, bounding box, segmentation map, and reference image [5, 9, 27, 42, 48, 50, 56, 60, 84, 88]. Another line of work improves the existing text conditioning [7, 17, 23], constrains internal features [6, 75], or augments it through rich text editor [25]. However, these works aim to create a single correct image by directly constraining the output space of solutions. In contrast, we offer a complementary approach – we allow users to pick and choose exactly what they want from multiple generated images, giving them more fine-grained control without relying solely on the model to create a single perfect image in one shot.

**Image blending** aims to combine multiple images in a seamless manner [13, 22, 59, 73]. Our work draws inspiration from Interactive Digital Photomontage [1], a seminal work that employs graph cut [10, 11, 44, 62] for blending multiple images given sparse user strokes. This method allows us to “capture the moment” [18] or create new visual effects. Many other works also use graph-cut optimization for textures [45] and videos [63]. Our method follows these graph-cut frameworks but performs the optimization in diffusion feature space, which captures more semantic information compared to pixel colors or edges. More recent image blending methods use generative models like GANs [79, 83] or diffusion models [4, 4, 8, 47, 64, 67, 72]. However, our method is specifically designed for compositing a spatially aligned image stack and is better at preserving user-selected

regions and blending them harmoniously. We also provide additional support for multi-image segmentation with sparse user strokes.

### 3. Method

Our method takes in a stack of generated images and produces a final image based on sparse user strokes. In our image stack, images are generated through ControlNet [84], using one or more prompts (Figure 2a). The generated images share common spatial structures, as they are produced using the same input condition (e.g., edge maps or depth maps).

Upon browsing the image stack, the user selects desired objects and regions via broad brush strokes on the images. For example, in Figure 2b, the user wishes to remove the rock at the Apple bite in the first image and add the red leaf from the third image. To do so, the user draws strokes on the base rock in the first image, the patch of grass in the second image, and the red leaf in the third image. Our algorithm takes the user input and performs a multi-label graph cut optimization in feature space to find a segmentation of image regions across the stack that minimizes seams. Finally, using a new injection scheme, our method composites the segmented regions during the denoising process (Figure 2c). The final composite image seamlessly blends the user-selected regions while faithfully preserving the local appearances.

Below, we first give a brief overview of image space graph-cut segmentation in Section 3.1, and then introduce our feature-based multi-image segmentation (Section 3.2) and blending algorithms (Section 3.3) in more detail.

### 3.1. Preliminaries: Segmentation with Graph Cut

Graph cut [10, 11, 44] has been widely used in several image synthesis and analysis tasks, including texture synthesis [45], image synthesis [1], segmentation [62], and stereo [77].

Here, we describe multi-label graph cut in image space [1, 11]. Suppose we have an image stack of  $N$  images, labeled 1 to  $N$ . For each 2D pixel location  $p$  in the output image  $I_o$ , the goal is to assign an image label  $i \in [1\dots N]$ . If a pixel  $I_o(p)$  in the output image is assigned the image label  $i$ , then  $I_o(p) = I_i(p)$ . The optimization seeks to find an optimal image label assignment for all output pixels such that a given energy cost function is minimized. We can define the energy cost function to encourage the label assignments to have desired properties, such as placing seams in less noticeable regions. An output image of size  $(W, H)$  means the optimization has to solve for  $W \times H$  variables, where each variable has  $N$  candidate labels. To solve the optimization, researchers have adopted max-flow min-cut algorithms for binary cases ( $N = 2$ ) [24], or  $\alpha$ -expansion for multi-label cases ( $N > 2$ ) [11].

### 3.2. Segmentation with Feature-Space Graph Cut

Given user strokes, our goal is to find a segmentation across the generated image stack and select image regions that adhere to the user strokes while minimizing seams. To achieve this, we also employ a multi-label graph cut optimization.

However, in contrast to prior image-space graph cut approaches [1, 11], we perform the optimization in feature space, using the key features  $K \in \mathbb{R}^{w \times h \times d}$  from the self-attention layers of the diffusion model.  $K$  serves as a compact, lower-resolution representation of the generated image, where  $(w, h)$  are smaller than the original image resolution  $(W, H)$  and  $d$  is the number of hidden dimensions. Prior works show that these features capture rich appearance and semantic information of the generated image [2, 14], which makes them better candidates than raw pixel values for finding good seams. Moreover, subsequent blending in feature space gives us more natural and seamless composites than in pixel space, without additional post-processing as in Agarwala et al. [1]. See Figure 3 for comparison.

Instead of solving for each pixel location  $(W, H)$ , our optimization assigns a label  $i \in [1\dots N]$  to each spatial location  $p = (x, y)$  in key features  $K$ , for  $x \in \{1\dots w\}$  and  $y \in \{1\dots h\}$ . During the blending stage, we use the label assignment to create composite self-attention features, which are then injected into ControlNet [84] to form the final result (Section 3.3).

As users generate the initial image stack, we store the query, key, and value features  $Q, K, V$  of each image for all layers and time steps on disk. After the user marks desired image regions with strokes, our system performs a multi-label graph cut using the stored key features  $K$  from the first encoding layer, where  $(w, h) = \frac{1}{8}(W, H)$ , at the final time

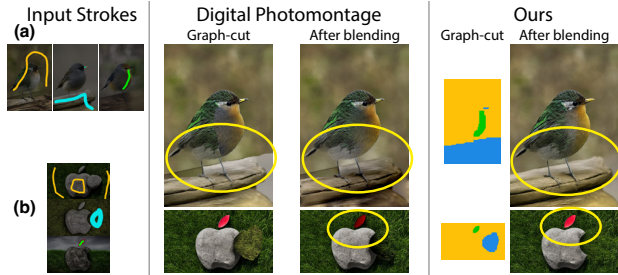


Figure 3. **Ours vs. Interactive Digital Photomontage** [1]. (a) Pixel-space graph cut may be more sensitive to low-level changes in color, whereas our diffusion feature-based graph cut selects seams that are more aligned with semantic features. (b) Due to large variations in color across the stack, gradient-domain blending [59] may alter local appearances, such as the red leaf.

step, when the generated content is mostly formed.

**Energy cost.** To create a good composite, we design the energy cost function to ensure that the label assignment 1) satisfies user-designated strokes and 2) picks good (unnoticeable) seams to join regions from different images. The energy function is composed of unary and pairwise costs [10, 11, 44]:

$$E_{\text{total}}(L) = \sum_p E(p, L_p) + \sum_{p,q} E(p, q, L_p, L_q), \quad (1)$$

where  $p$  and  $q$  are neighboring spatial locations in key features  $K$ .  $L_p$  and  $L_q$  are image labels to be optimized.

**Unary term.** Unary costs are the cost of assigning a label  $L_p$  at feature location  $p$ . Here, we assign a high penalty if there is a user stroke at the corresponding pixel location of  $p$ , and the label is not the image that the user has designated:

$$E(p, L_p) = \begin{cases} C & \text{if } S(p, i) = 1 \text{ and } L_p \neq i \\ 0 & \text{otherwise,} \end{cases} \quad (2)$$

where  $S(p, i)$  is an indicator function of whether there is a user stroke at the corresponding pixel location of  $p$  in image  $i$ , and  $C$  is a large constant. We use  $C = 10^6$  in our results.

**Pairwise term.** Pairwise costs are the cost of assigning neighboring feature locations a pair of labels. Because we want seams to be less noticeable, we encourage seams to fall on edges (lower cost), where the neighboring features are significantly different:

$$E(p, q, L_p, L_q) = \begin{cases} \sum_{i=1}^N \lambda e^{-\frac{|f_i(p) - f_i(q)|}{2\sigma}} & \text{if } L_p \neq L_q \\ 0 & \text{otherwise,} \end{cases} \quad (3)$$

where  $f_i(p)$  is a feature vector derived from the key features  $K$  of image  $i$  at location  $p$ . To capture the most important features,  $f_i(p)$  consists of the top-10 PCA components of  $K$  at location  $p$ , computed across hidden dimensions and heads.

The cost is low if the features of  $p$  and  $q$  are dissimilar for all images within the stack; in other words, we encourage seams where  $p$  and  $q$  straddle an edge in all the images.  $\sigma$  controls how quickly the penalty falls off as feature distance increases, and  $\lambda$  is a constant scale for the cost range. We use  $\lambda = 100$  and  $\sigma = 10$  in all our results.

**Discussion.** While it is possible to segment each image individually using off-the-shelf methods (e.g., SAM [43]), it often creates conflicts across the image stack where objects overlap, requiring extra user intervention to resolve conflicts. Instead, our multi-label graph cut optimization can automatically account for all images within the stack, assigning a unique label to each location.

### 3.3. Composition with Self-Attention Feature Injection

The above optimization gives us an image label assignment per feature location for the output image. We use this assignment to make composite features  $Q^{\text{comp}}$ ,  $K^{\text{comp}}$  and  $V^{\text{comp}}$  from the respective features  $Q$ ,  $K$ ,  $V$  of the image stack, for each self-attention layer in ControlNet. We then inject these composite features  $Q^{\text{comp}}$ ,  $K^{\text{comp}}$  and  $V^{\text{comp}}$  into ControlNet to form the final result.

When users input strokes, they designate one image within the stack as the base image (usually the one whose background region is selected). During the blending stage, we use the seed and prompt of this base image when injecting the composite features.

Specifically, we resize the label assignment map  $L$  into the respective sizes of each self-attention layer  $l$ . Then, we make composite features  $Q^{\text{comp}}$ ,  $K^{\text{comp}}$  and  $V^{\text{comp}}$  as follows:

$$Q_l^{\text{comp}} = M_l^B \odot Q_l^{\text{model}} + \sum_{i \neq B} M_l^i \odot Q_l^i, \quad (4)$$

$$K_l^{\text{comp}} = \sum_i M_l^i \odot K_l^i, \quad (5)$$

$$V_l^{\text{comp}} = \sum_i M_l^i \odot V_l^i, \quad (6)$$

where  $M_l^i$  is the binary mask of feature locations with the label assignment  $i$ , resized to layer  $l$ .  $M^B$  represents the mask of the base image, where  $B$  is the base image index.  $Q_l^i$  are the query features  $Q$  from image  $i$  at layer  $l$  (stored during initial generation), and similarly for  $K_l^i$  and  $V_l^i$ .  $Q^{\text{model}}$  are the query features generated from the model during the blending stage, which are different from those during the initial generation. These composite features are injected into the U-Net’s self-attention maps for all layers and time steps.

Note that we inject the initially generated self-attention features for all images *except* for  $Q^B$ , the query features of the base image. If we inject the initial  $Q^B$  features, we often observe suboptimal blending at the seams. As noted in

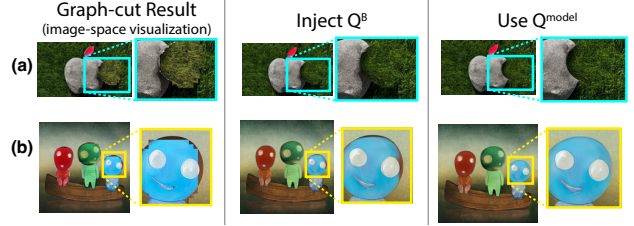


Figure 4. **Using  $Q^B$  vs.  $Q^{\text{model}}$ .**  $Q^B$ : query features of the base image from initial generation.  $Q^{\text{model}}$ : query features generated from the model during the blending stage. Leftmost column: visualization of diffusion-feature graph cut results, resized to image dimensions and combined in image space. (a) Injecting  $Q^B$  does not leave room for the model to adapt its image structure near seams, causing the shadow from the input image to remain. (b) Injecting  $Q^B$  causes the image to strictly adhere to low-resolution graph cut boundaries, whereas using  $Q^{\text{model}}$  adjusts the boundaries to align with semantic features in high-resolution image space.

previous literature [2, 14],  $Q$  influences the image structure, while  $K$  and  $V$  influence the appearance. Hence, injecting  $Q^B$  (and thus completely overwriting the  $Q$  features) eliminates the opportunity for the model to adapt the image structure near the seams. Allowing  $Q$  within the mask  $M^B$  to change over time allows the model to adapt to the different graph-cut regions when blending (Figure 4a). It also adjusts the low-resolution graph cut boundaries to align with semantic features in high-resolution pixel space (Figure 4b).

## 4. Results

By supporting the ability to combine generated images, our method allows users to achieve a wider range of results with more flexibility and control. Here, we highlight some use cases and show compelling results for each application. We create the examples using various pre-trained ControlNet models [84] with Stable Diffusion 1.5, such as canny edge, scribble map, Openpose [15], and depth map. Please see Appendix A and E for additional results and details.

**Appearance Mixing.** First, we show applications in creative and artistic design, where users refine images based on subjective preference. This is useful in cases where the user may not realize what they want until they see it (e.g., creative exploration). For example, users may use our method for exploring architectural designs, e.g., by combining the roofs, windows, and doors from different images (Figures 5a) or adding features such as a rooftop canon or a glowy courtyard (Figure 5b). Additionally, users can composite different components to create something new. For example, we can combine the body, ear, and arm of a robot to form a new robot (Figure 5e). This strategy can also be applied to other subjects, e.g., to combine new colors in a bird’s feathers (Figure 5d, 15) or a snake’s scales (Figure 5c).

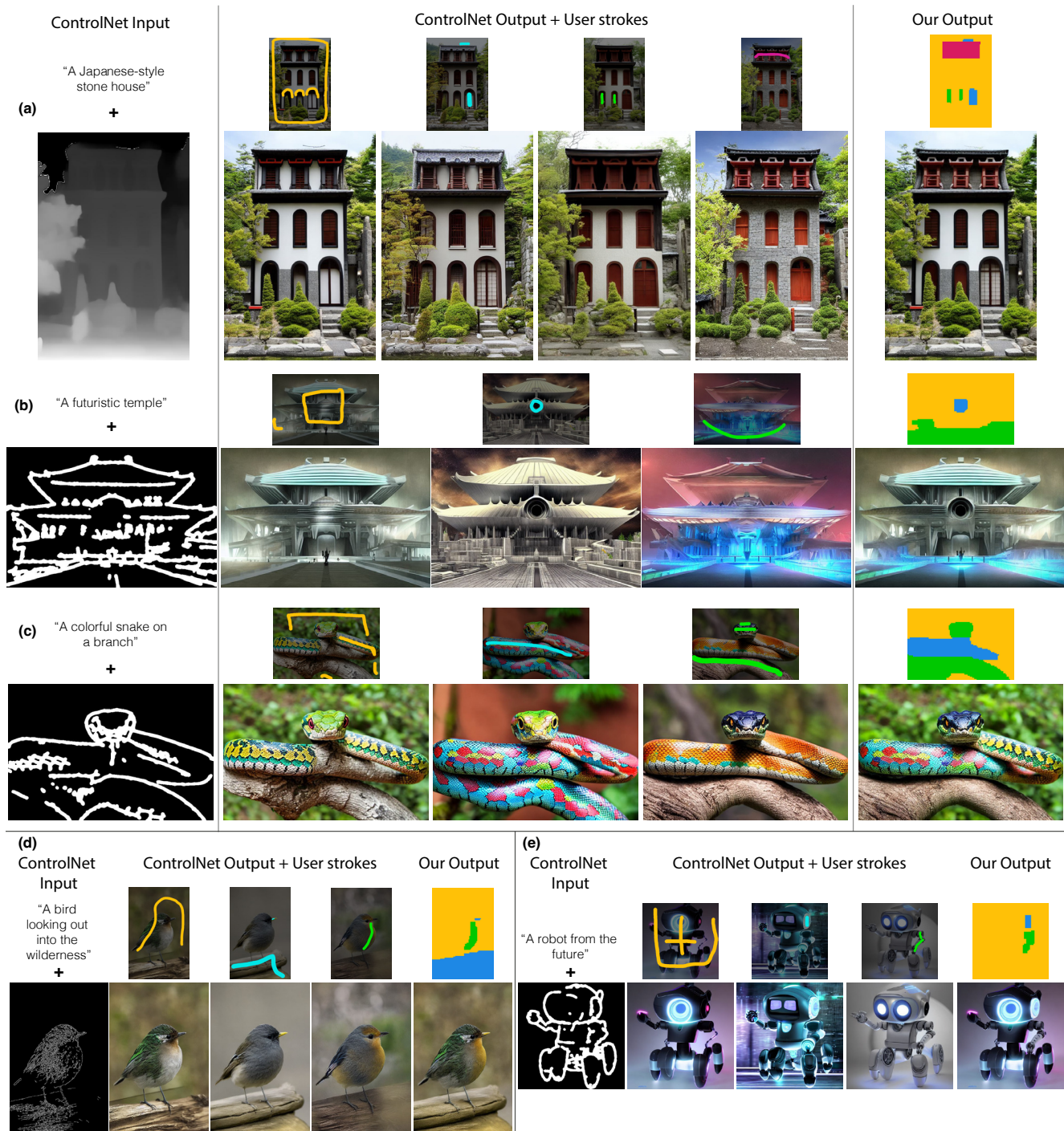


Figure 5. **Appearance Mixing Results.** Examples of using Generative Photomontage for creative exploration. (a, b) Users can combine different architectural elements (e.g., roof, windows, door) to form new architectural designs. (c) The user combines different colors of snakes to create a striking image. (d) The user selects the yellow beak from the second image and combines different vibrant colors in a bird’s feather to explore new looks. (e) The user combines different parts of a futuristic robot to form their favorite look.

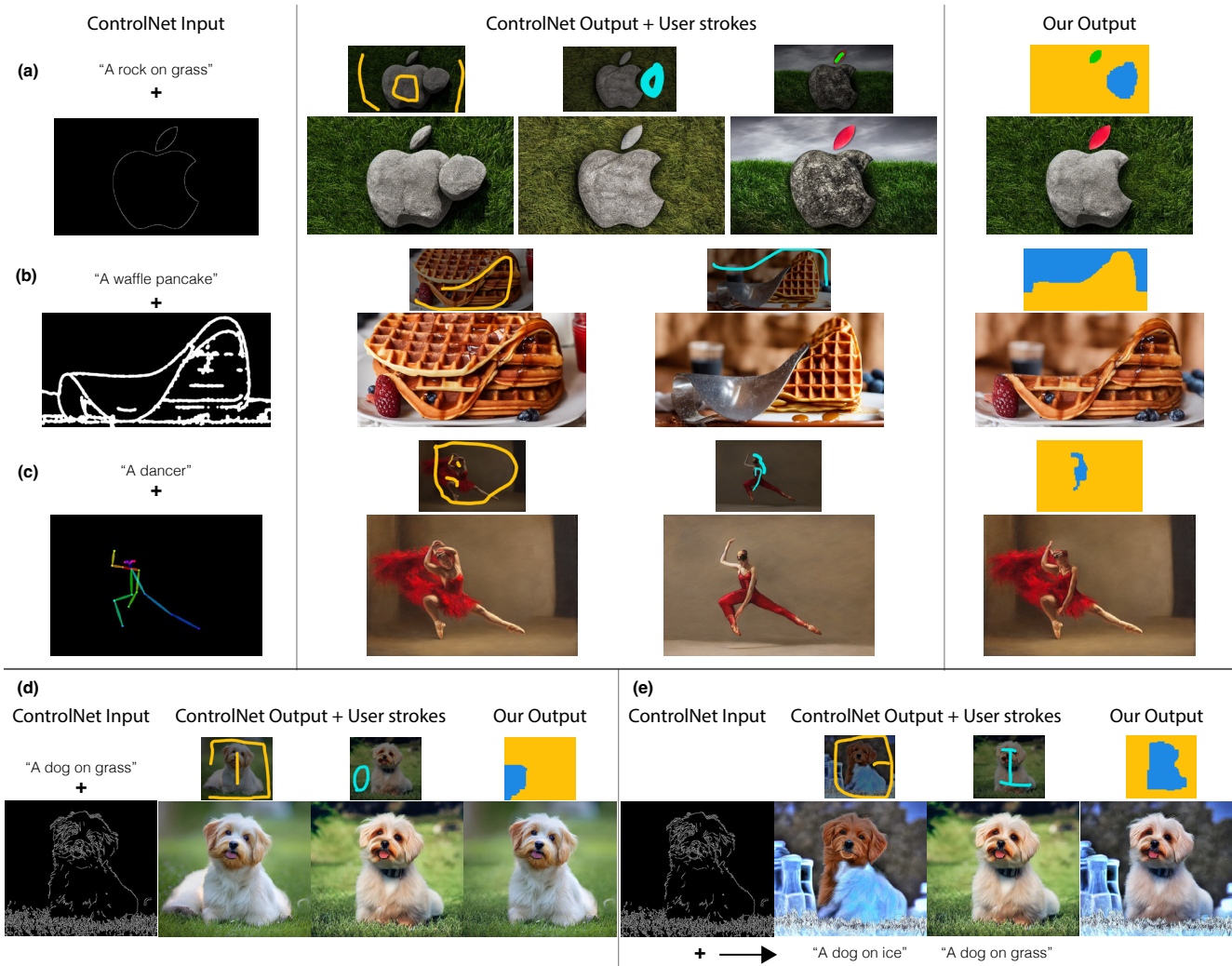


Figure 6. **Shape and Artifacts Correction Results.** Our method can fix incorrect shapes and artifacts from ControlNet’s outputs, which often occur for uncommon input shapes. For example, (a) users can remove the extra rock at the Apple bite with a patch of grass from the second image, and (b) correct the shape and contour of the first waffle by selecting the background region of the second image. Users can also (c) correct the dancer’s pose, (d) remove the extra leg of the dog, and (e) and replace the first dog with artifacts with the second dog.



Figure 7. **Prompt Alignment.** Our method can be used to increase alignment to long, complicated prompts. (a) Example where vanilla ControlNet’s outputs do not adhere to the prompt. (b) With Generative Photomontage, users can create the desired image by combining the outputs from shorter, simpler prompts.

**Shape and Artifacts Correction.** While users can provide a sketch to guide ControlNet’s output, ControlNet may fail to adhere to the user’s input condition, especially when asked to generate objects with uncommon shapes. In such cases, our method can be used to “correct” object shapes and scene layouts, given a replaceable image patch within the stack.

For example, suppose the user wishes to create an Apple-logo-shaped rock and prompts ControlNet with “A rock on grass” alongside an Apple-logo sketch. Since Apple-logo-shaped rocks are not commonly seen in real life (and thus out-of-training distribution), the model fails to produce the desired image. Figure 6a shows an additional rock piece covering the apple bite. To correct it, the user can use our framework to replace it with a patch of grass from another image in the stack (Figure 6a). Similarly, users can correct ControlNet’s output to create waffles in the shape of famous architectural buildings (Figure 6b), which is difficult to achieve with ControlNet alone due to the rare object-shape combination. Finally, we show other correction examples, such as a dancer with an incorrect pose (Figure 6c) and a dog with an extra leg (Figure 6d). Figure 6e shows an example of replacing an unrealistic-looking dog with a different one.

**Prompt Alignment.** In addition, our method can be used to increase prompt alignment in cases where the generated output does not accurately follow the input prompt. For example, it is difficult for ControlNet to follow all aspects of long complicated prompts, such as “A red fairy, a green fairy, and a blue fairy sitting from left to right in a brown boat” (Figure 7a). Using our method, users can create the desired image by breaking it up into simpler prompts and selectively combining the outputs (Figure 7b). Since our results depend on the availability of at least one “correct” candidate per region within the generated stack, we encourage our method to be used in conjunction with existing methods [17, 23] for greater accuracy and control.

## 5. Evaluation

Our graph cut runs in  $\sim 1$  sec, and the blending stage takes about 7-13 seconds on an NVIDIA A6000 GPU for 2-5 images (of sizes  $512 \times 512$  to  $1024 \times 512$ ). For reference, one forward pass of vanilla ControlNet takes 7-17 sec for a batch of 5 images. Storage space for the initially generated  $QKV$  features depends on image resolution and is  $\sim 2$ GB for a  $512 \times 512$  image. To save storage space, one could store a subset of features with a trade-off of lower appearance fidelity. Please see Appendix C.2 for more details.

Below, we compare our method against baselines on the examples from Section 4, which spans various use cases.

### 5.1. Segmentation

We compare our multi-label graph cut with a modified version of SAM [43] as well as the pixel-space graph cut in

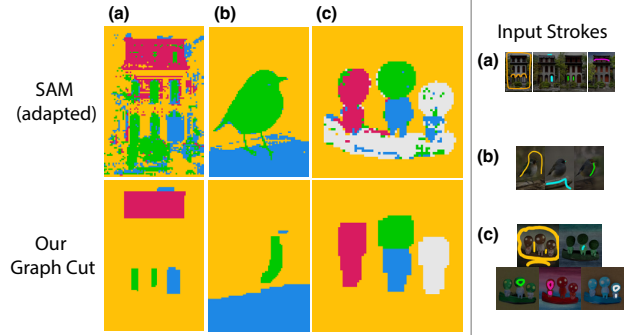


Figure 8. **Our Graph Cut vs. SAM [43].** We adapt SAM to an image stack as follows: first, we run SAM on each image, using the user strokes as positive and negative samples. Then, for each pixel location, we choose the image label with the largest logit score. As shown, SAM may output noisy, incongruent labels within an object, such as the building (a) and fairies (c). SAM may also fail to follow user strokes, such as the bird interior (b) and the boat (c). Our graph cut takes into account the entire image stack during optimization and outputs labels that are congruent and satisfy user strokes.

Interactive Digital Photomontage [1]. Please see Appendix C.1 for an ablation of features used in our graph cut.

**SAM.** Because SAM is trained to segment a single image, it is not straightforward to adapt it to a multi-image stack while maintaining coverage and avoiding overlaps. As a baseline, we use the following setup: given an image stack, we run SAM on each image with the user strokes as positive and negative samples. SAM outputs logits per pixel per image. For each pixel, we assign the image label with the largest logit score. As shown in Figure 8, the output labels have two major types of artifacts: 1) incongruent (noisy) labels within an object; 2) the segmentation does not follow user strokes.

**Interactive Digital Photomontage.** We compare our feature-based graph cut with their pixel-space counterpart. Specifically, we use their “match edge” seam objective, where the pairwise term  $E(p, q, L_p, L_q)$  is computed based on a Sobel filter on the RGB values. As shown in Figure 3, the edge strength computed from the filter may be sensitive to low-level changes in color, which could cause their graph cut to select seams that fall on undesired edges. Diffusion feature-based graph cut, on the other hand, selects seams that are more aligned with semantic features. Moreover, as diffusion features are lower resolution than the original images, our graph-cut optimization is more efficient, with  $1/64$  the number of variables.

### 5.2. Blending

For blending, we consider overall realism and local fidelity of user-selected regions. First, we qualitatively compare our results with several baselines:



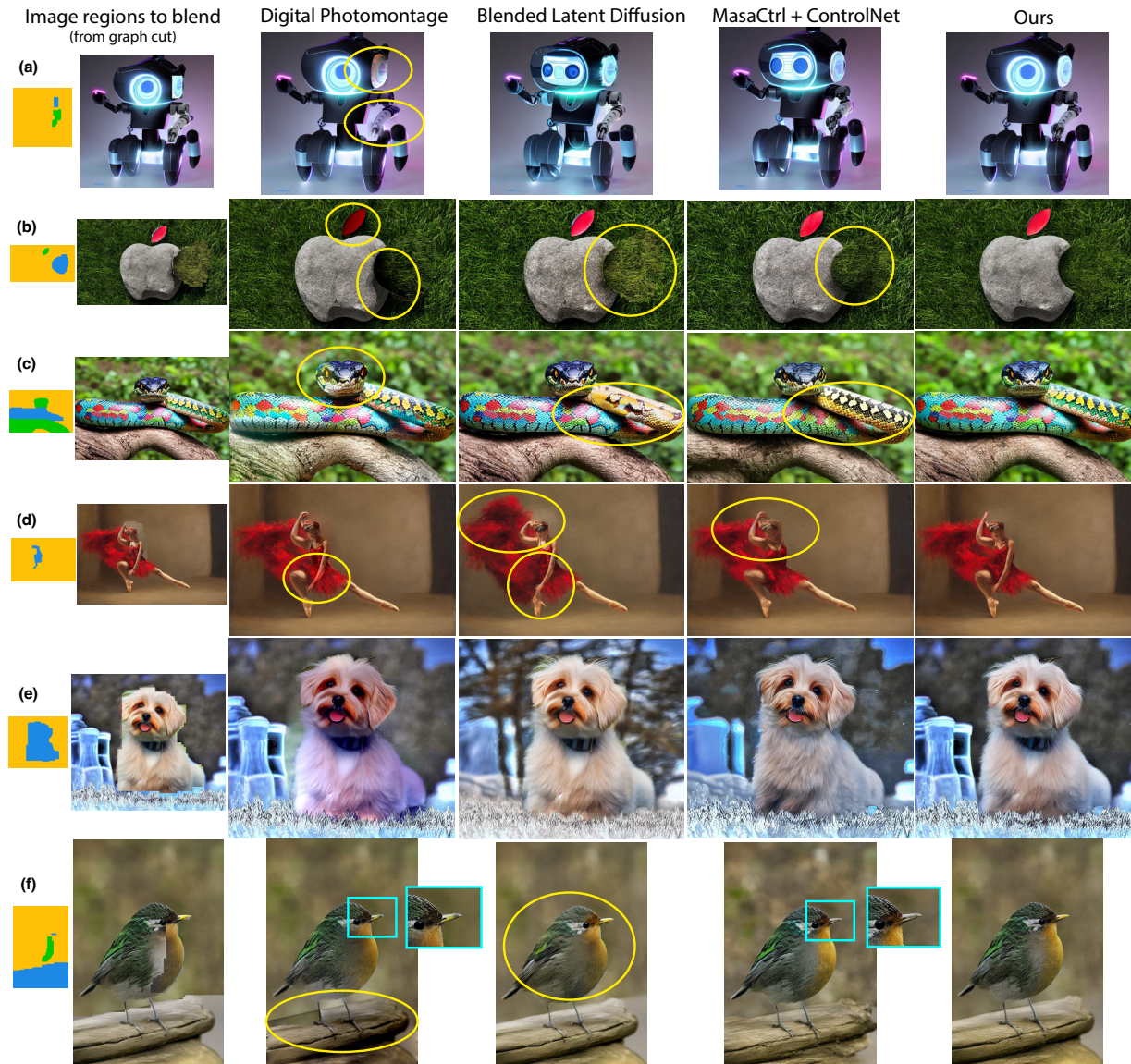


Figure 9. **Qualitative Comparison.** Leftmost column: Image regions to blend (output of graph-cut optimization). Graph-cut in diffusion feature space is visualized on the left, and the image-space composite of that graph-cut is visualized on the right. Interactive Digital Photomontage [1]: pixel-space graph-cut may cause seams to fall on undesired edges (see Figure 3 for details), and their gradient-domain blending often fails to preserve color, e.g., the bird’s yellow beak is not preserved in (f). Blended latent diffusion [4] and MasaCtrl+ControlNet [14] may lead to color changes (c, f) and structure changes (a, b, d, e).

|                                                           | Ours         | Interactive Digital Photomontage | Blended Latent Diffusion | BLD + MultiDiffusion | MasaCtrl + ControlNet | Cross-Domain Compositing | Deep Image Blending | GP-GAN       | Collage Diffusion |
|-----------------------------------------------------------|--------------|----------------------------------|--------------------------|----------------------|-----------------------|--------------------------|---------------------|--------------|-------------------|
| Masked LPIPS ↓                                            | 0.104        | <b>0.085</b>                     | 0.187                    | 0.188                | 0.198                 | 0.380                    | 0.252               | 0.220        | 0.244             |
| PSNR ↑                                                    | <b>23.44</b> | 21.12                            | <u>21.17</u>             | 20.66                | 19.50                 | 20.31                    | 18.35               | 18.11        | 20.95             |
| Seam Gradient Score<br>min: 0.256, avg: 0.337, max: 0.427 | 0.335        | 0.312                            | 0.386                    | 0.326                | 0.341                 | 0.394                    | 0.301               | <i>0.207</i> | <i>0.487</i>      |

Table 1. **Quantitative Results.** To measure fidelity of local image regions, we report masked LPIPS and PSNR. To measure blending quality of seams, we compute a seam gradient score (SG), which is the mean gradient magnitude along seams that join different image regions. For reference, we also compute the minimum, average, and maximum SG scores of each image stack and report their averages on the left. Methods with SG scores that fall outside of this range exhibit significant seam artifacts (italicized).

**Pixel-Space Photomontage.** Interactive Digital Photomontage (IDP) uses Poisson blending [59] as a post-process for smoothing composite regions together. Because generated images [59] tend to have wide color variations, gradient-domain blending often leads to changes in color, such as the marked regions in Figure 9. Our method is better at preserving local color and image appearances.

**Noise-based Blending.** Blended Latent Diffusion (BLD) [4] blends images by combining their noise at each diffusion step. For this baseline, we inject the noises of image  $i = 2 \dots N$  into the noise of the base image  $i = 1$ . As shown in Figure 9, BLD may change the appearance of the base image (a, c, e), the injected regions (d), and include artifacts (b, e, f). We also experiment with fusing the noises with greater overlap, inspired by MultiDiffusion [8], but they lead to more artifacts at the seams (see Appendix B).

**Attention-based Editing.** We also compare our method with an adapted version of MasaCtrl [14] with ControlNet. We adapt their mask-guided framework by designating the base image as the target image and the other images within the stack as source images. We extend their framework to use multiple foreground masks (one for each image beyond the base image). As shown in Figure 9, this may change the appearance of the base image (a, c, e), selected regions (d, e, f), or show other blending artifacts (b).

**Other Blending.** We compare our method against other diffusion-based methods, such as CollageDiffusion [64] and Cross-Domain Compositing [29]. However, these methods fail to preserve local appearance when blending different regions. We also compare with GP-GAN [79] and Deep Image Blending [83], which show artifacts in blended regions. Please see Appendix B for the qualitative results and additional baselines.

**Quantitative Metrics.** To measure local appearance fidelity, we computed masked LPIPS [85] and PSNR [33]. For LPIPS, we use the masks from our feature-based graph cut, resized to image dimensions. For PSNR, we compare each blended result with the image-space composite (also created with the graph cut masks). Note that the image-space composites contain noticeable seams (e.g., the first column in Figure 9) and only serve as a proxy in the absence of groundtruth data.

To measure seam artifacts, we compute the average gradient magnitude along seams, called the seam gradient (SG) score. Since some seams fall on object boundaries, the gradient is not expected to be zero. Rather, it should be within range of the SG scores of images in the stack. For reference, we compute the minimum, average, and maximum SG scores of each image stack and report their averages in Table 1.

**Quantitative Results.** As shown in Table 1, our method achieves the highest PSNR score and the second lowest LPIPS loss across all the baselines. Our method’s SG score

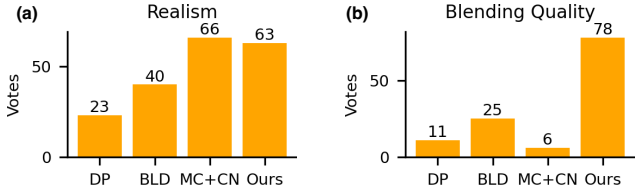


Figure 10. **User Survey Results.** Across 12 test scenes, we asked participants to select the best image out of four: Interactive Digital Photomontage (DP), Blended Latent Diffusion (BLD), MasaCtrl+ControlNet (MC+CN), and Ours. The results suggest that our method has the best blending quality by a wide margin while being comparable to MasaCtrl+ControlNet in realism.

is within range and close to the average SG score. CollageDiffusion has a large SG score due to major seam artifacts, and GP-GAN has a low SG score because the images are significantly faded with a reduced color range. Please see Appendix B for additional examples. Deep Image Blending and Cross-Domain Compositing have relatively large LPIPS losses. BLD has the second-highest PSNR score and performs better than its variant, BLD+MultiDiffusion.

**User Survey.** Finally, we conduct two user surveys to compare our results with the most competitive baseline in each domain: Interactive Digital Photomontage (pixel-space), BLD (noise-based), and MasaCtrl+ControlNet (attention-based). For each test scene, we ask participants to select the best image out of four: (1) Which image appears most realistic to you? and (2) Which image is the best at blending all the selected regions? Results show that our method is comparable to MasaCtrl+ControlNet in terms of realism but has the best blending quality among the baselines by a wide margin (Figure 10).

### 5.3. Ablation Study

Here, we ablate our self-attention injection scheme with alternative injection strategies [2, 14, 31], adapted to our use case. In these comparisons, we use the same graph cut segmentation as input.

First, we consider using shared (concatenated) key and value features, i.e.  $K^{\text{concat}} = [K^1, K^2, \dots, K^N]$  and  $V^{\text{concat}} = [V^1, V^2, \dots, V^N]$ , which Hertz et al. [31] used to transfer style across different images. Figure 11 shows the results along with the feature-based graph cut, visualized in image space. As shown, the alternative injection schemes can change the local image appearance, such as the dog’s background, the robot’s head, the snake color, and the waffle. Our results align with the observation [2, 14] that  $Q$  features influence the image structure, and  $K$  and  $V$  features influence the image appearance.  $K^{\text{concat}}, V^{\text{concat}}$  allows  $Q$  features to match with keys that are not from the target image region and can thus result in appearance changes. Our method only makes the target image region’s keys and values available and, hence, is able to preserve local appearances.

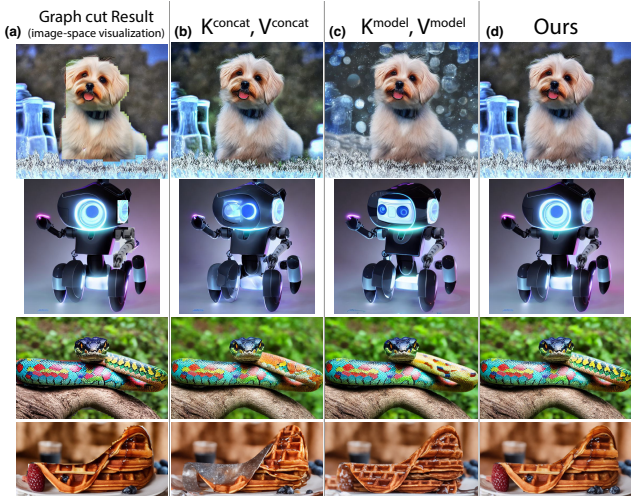


Figure 11. **Ablation with Alternative Self-Attention Injection Strategies.** (a) Input graph-cut segmentation, visualized here by resizing the diffusion-feature masks to match image dimensions and compositing in pixel space. (b) Inspired by StyleAligned [31], we replace  $K^{\text{comp}}, V^{\text{comp}}$  with  $K^{\text{concat}} = [K^1, K^2, \dots, K^N]$  and  $V^{\text{concat}} = [V^1, V^2, \dots, V^N]$ . (c) Similar to Equation 4, we inject  $K^{\text{model}}$  and  $V^{\text{model}}$  for the base image. (d) Our method can preserve local image appearances while harmoniously blending them.

Next, we consider using  $K^{\text{model}}$  and  $V^{\text{model}}$  for the base image, similar to Equation 4. Using  $K^{\text{model}}, V^{\text{model}}$  for the base image also allows appearances to change. By injecting  $K^B$  and  $V^B$  of the base image stored during initial generation, our method is able to preserve their appearance during blending. For additional ablations on graph cut features and attention injection parameters, please see Appendix C.

## 6. Discussion and Limitations

In this work, we proposed a new approach for generating images: by compositing it from multiple ControlNet-generated images. To this end, we introduced a novel method for segmenting and blending the images using their diffusion features, and we showed many compelling applications. At a broader level, our work suggests a new user workflow for interacting with text-to-image models: rather than trying to get the model to output the final end-product (i.e., a *single* image that contains everything the user wants), we treat the model’s output as *intermediate* outputs, from which users provide further input to create their final end-product. This approach not only gives users more fine-grained control over the final output, but also allows us to fully utilize the model’s generative capabilities in creating diverse candidates. We hope this work inspires new ways of interacting with generative models.

**Limitations.** While we have shown our method’s versatility in various applications, we also observe several limitations. First, our current graph cut parameters are empirically cho-

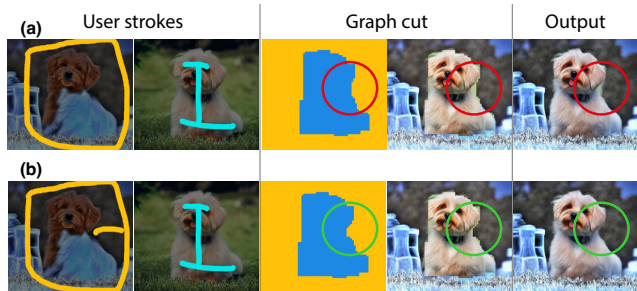


Figure 12. **Limitation.** Our graph cut optimization prefers smaller seam circumferences due to lower pairwise costs (Equation 3). For objects with curved outlines, users may need to refine boundaries with additional strokes. (a) Our graph cut over-segmented the dog at its neck region because a vertical seam (circled in red) has a lower circumference (and lower cost) than a curved one. (b) To refine the boundary, users can add an additional stroke in the background, which aligns the boundary to the dog’s neck (circled in green).

sen to encourage congruous regions, which penalizes seam circumference. While this works well for many cases, if the target object has a curvy outline, it may require additional user strokes to obtain a finer boundary (Figure 12). Since graph cut is solved in near real-time ( $\sim 1s$ ), users can quickly check the graph-cut result by visualizing it in image space and iterate as needed.

Second, our method assumes some spatial consistency among images in the stack. If the images differ significantly in scene structure, it will rely more on the user to select proper regions to form a valid scene (Figure 13a). Alternatively, users can increase spatial consistency by adding more structure to the input control (Figure 13b). Future work can investigate ways to relax spatial consistency constraints and automatically account for dramatic scene structure changes during segmentation and blending.

**Acknowledgments** We are grateful to Kangle Deng for his help with setting up the user survey. We also thank Maxwell Jones, Gaurav Parmar, and Sheng-Yu Wang for helpful comments and suggestions and Or Patashnik for initial discussions. This project is partly supported by the Amazon Faculty Research Award, DARPA ECOLE, the Packard Fellowship, and a joint NSFC-ISF Research Grant no. 3077/23.

## References

- [1] Aseem Agarwala, Mira Dontcheva, Maneesh Agrawala, Steven Drucker, Alex Colburn, Brian Curless, David Salesin, and Michael Cohen. Interactive digital photomontage. In *ACM SIGGRAPH*, 2004. 2, 3, 4, 8, 9, 17
- [2] Yuval Alaluf, Daniel Garibi, Or Patashnik, Hadar Averbuch-Elor, and Daniel Cohen-Or. Cross-image attention for zero-shot appearance transfer. In *ACM SIGGRAPH*, 2024. 2, 4, 5, 10, 17
- [3] Auguste08. Kodama princess mononoke 3d print model. See source, 2023. 18



Figure 13. **Limitation.** Our method assumes some spatial consistency among images in the stack. In cases where the images differ significantly in scene structure, our method may produce semantically incorrect outputs. (a) Two images have different horizons in the background. Naively combining two halves of the images leads to an inconsistent horizon (bottom left, circled red). Users can manually designate a consistent horizon by selecting the background of the second image (bottom, middle). (b) Alternatively, users can add a horizon in the input sketch to ControlNet to make it consistent across both images.

- [4] Omri Avrahami, Ohad Fried, and Dani Lischinski. Blended latent diffusion. *ACM Transactions on Graphics (TOG)*, 42(4), 2023. 3, 9, 10, 16, 17, 20
- [5] Omri Avrahami, Thomas Hayes, Oran Gafni, Sonal Gupta, Yaniv Taigman, Devi Parikh, Dani Lischinski, Ohad Fried, and Xi Yin. Spatext: Spatio-textual representation for controllable image generation. In *IEEE Conference on Computer Vision and Pattern Recognition (CVPR)*, 2023. 3
- [6] Omri Avrahami, Amir Hertz, Yael Vinker, Moab Arar, Shlomi Fruchter, Ohad Fried, Daniel Cohen-Or, and Dani Lischinski. The chosen one: Consistent characters in text-to-image diffusion models. In *ACM SIGGRAPH*, 2024. 3
- [7] Zhipeng Bao, Yijun Li, Krishna Kumar Singh, Yu-Xiong Wang, and Martial Hebert. Separate-and-enhance: Compositional finetuning for text-to-image diffusion models. In *ACM SIGGRAPH*, 2024. 3
- [8] Omer Bar-Tal, Lior Yariv, Yaron Lipman, and Tali Dekel. Multidiffusion: Fusing diffusion paths for controlled image generation. In *International Conference on Machine Learning (ICML)*, 2023. 3, 10, 16, 20
- [9] Shariq Farooq Bhat, Niloy Mitra, and Peter Wonka. Loosecontrol: Lifting controlnet for generalized depth conditioning. In *ACM SIGGRAPH 2024 Conference Papers*, pages 1–11, 2024. 3
- [10] Yuri Boykov and Vladimir Kolmogorov. An experimental comparison of min-cut/max-flow algorithms for energy minimization in vision. *IEEE Transactions on Pattern Analysis and Machine Intelligence (TPAMI)*, 26(9), 2004. 3, 4
- [11] Yuri Boykov, Olga Veksler, and Ramin Zabih. Fast approximate energy minimization via graph cuts. *IEEE Transactions on Pattern Analysis and Machine Intelligence (TPAMI)*, 23(11), 2001. 3, 4
- [12] Tim Brooks, Aleksander Holynski, and Alexei A Efros. Instructpix2pix: Learning to follow image editing instructions. In *IEEE Conference on Computer Vision and Pattern Recognition (CVPR)*, 2023. 2
- [13] Peter J Burt and Edward H Adelson. The laplacian pyramid as a compact image code. In *Readings in computer vision*. 1987. 3
- [14] Mingdeng Cao, Xintao Wang, Zhongang Qi, Ying Shan, Xiaohu Qie, and Yinqiang Zheng. Masactrl: Tuning-free mutual self-attention control for consistent image synthesis and editing. In *IEEE International Conference on Computer Vision (ICCV)*, 2023. 2, 4, 5, 9, 10, 17, 23
- [15] Z. Cao, G. Hidalgo Martinez, T. Simon, S. Wei, and Y. A. Sheikh. Openpose: Realtime multi-person 2d pose estimation using part affinity fields. *IEEE Transactions on Pattern Analysis and Machine Intelligence (TPAMI)*, 2019. 5
- [16] Huiwen Chang, Han Zhang, Jarred Barber, AJ Maschinot, Jose Lezama, Lu Jiang, Ming-Hsuan Yang, Kevin Murphy, William T Freeman, Michael Rubinstein, et al. Muse: Text-to-image generation via masked generative transformers. In *International Conference on Machine Learning (ICML)*, 2023. 2
- [17] Hila Chefer, Yuval Alaluf, Yael Vinker, Lior Wolf, and Daniel Cohen-Or. Attend-and-excite: Attention-based semantic guidance for text-to-image diffusion models. *ACM Transactions on Graphics (TOG)*, 42(4), 2023. 2, 3, 8
- [18] Michael F Cohen and Richard Szeliski. The moment camera. *Computer*, 39(8), 2006. 3
- [19] Heidi Cross. See source, 2021. 18
- [20] Prafulla Dhariwal and Alexander Nichol. Diffusion models beat gans on image synthesis. In *Conference on Neural Information Processing Systems (NeurIPS)*, 2021. 2
- [21] Patrick Esser, Sumith Kulal, Andreas Blattmann, Rahim Entezari, Jonas Müller, Harry Saini, Yam Levi, Dominik Lorenz, Axel Sauer, Frederic Boesel, et al. Scaling rectified flow transformers for high-resolution image synthesis. In *International Conference on Machine Learning (ICML)*, 2024. 2
- [22] Zeev Farbman, Gil Hoffer, Yaron Lipman, Daniel Cohen-Or, and Dani Lischinski. Coordinates for instant image cloning. *ACM Transactions on Graphics (TOG)*, 28(3), 2009. 3
- [23] Weixi Feng, Xuehai He, Tsu-Jui Fu, Varun Jampani, Arjun Akula, Pradyumna Narayana, Sugato Basu, Xin Eric Wang, and William Yang Wang. Training-free structured diffusion

- guidance for compositional text-to-image synthesis. In *International Conference on Learning Representations (ICLR)*, 2023. [2](#), [3](#), [8](#)
- [24] Lester Randolph Ford and Delbert R Fulkerson. A simple algorithm for finding maximal network flows and an application to the hitchcock problem. *Canadian journal of Mathematics*, 9, 1957. [4](#)
- [25] Songwei Ge, Taesung Park, Jun-Yan Zhu, and Jia-Bin Huang. Expressive text-to-image generation with rich text. In *IEEE International Conference on Computer Vision (ICCV)*, 2023. [3](#)
- [26] Jing Gu, Yilin Wang, Nanxuan Zhao, Wei Xiong, Qing Liu, Zhifei Zhang, He Zhang, Jianming Zhang, HyunJoon Jung, and Xin Eric Wang. Swapanything: Enabling arbitrary object swapping in personalized visual editing. *arXiv preprint arXiv:2404.05717*, 2024. [2](#)
- [27] Zeqi Gu, Ethan Yang, and Abe Davis. Filter-guided diffusion for controllable image generation. In *ACM SIGGRAPH*, 2024. [3](#)
- [28] Julian Jorge Andrade Guerreiro, Mitsuru Nakazawa, and Björn Stenger. Pct-net: Full resolution image harmonization using pixel-wise color transformations. In *IEEE Conference on Computer Vision and Pattern Recognition (CVPR)*, 2023. [16](#), [21](#)
- [29] Roy Hachnochi, Mingrui Zhao, Nadav Orzech, Rinon Gal, Ali Mahdavi-Amiri, Daniel Cohen-Or, and Amit Haim Bermano. Cross-domain compositing with pretrained diffusion models. *arXiv preprint arXiv:2302.10167*, 2023. [10](#), [16](#), [21](#)
- [30] Amir Hertz, Ron Mokady, Jay Tenenbaum, Kfir Aberman, Yael Pritch, and Daniel Cohen-Or. Prompt-to-prompt image editing with cross attention control. In *International Conference on Learning Representations (ICLR)*, 2023. [2](#)
- [31] Amir Hertz, Andrey Voynov, Shlomi Fruchter, and Daniel Cohen-Or. Style aligned image generation via shared attention. In *IEEE Conference on Computer Vision and Pattern Recognition (CVPR)*, 2024. [2](#), [10](#), [11](#)
- [32] Jonathan Ho, Ajay Jain, and Pieter Abbeel. Denoising diffusion probabilistic models. In *Conference on Neural Information Processing Systems (NeurIPS)*, 2020. [2](#)
- [33] Alain Hore and Djemel Ziou. Image quality metrics: Psnr vs. ssim. In *International Conference on Pattern Recognition (ICPR)*, 2010. [10](#)
- [34] Nisha Huang, Weiming Dong, Yuxin Zhang, Fan Tang, Ronghui Li, Chongyang Ma, Xiu Li, and Changsheng Xu. Creativesynth: Creative blending and synthesis of visual arts based on multimodal diffusion. *arXiv preprint arXiv:2401.14066*, 2024. [2](#)
- [35] Wenjing Huang, Shikui Tu, and Lei Xu. Pfb-diff: Progressive feature blending diffusion for text-driven image editing. *arXiv preprint arXiv:2306.16894*, 2023. [2](#)
- [36] Justin Johnson, Alexandre Alahi, and Li Fei-Fei. Perceptual losses for real-time style transfer and super-resolution. In *European Conference on Computer Vision (ECCV)*, 2016. [17](#)
- [37] Minguk Kang, Jun-Yan Zhu, Richard Zhang, Jaesik Park, Eli Shechtman, Sylvain Paris, and Taesung Park. Scaling up gans for text-to-image synthesis. In *IEEE Conference on Computer Vision and Pattern Recognition (CVPR)*, 2023. [2](#)
- [38] Tero Karras, Miika Aittala, Timo Aila, and Samuli Laine. Elucidating the design space of diffusion-based generative models. In *Conference on Neural Information Processing Systems (NeurIPS)*, 2022. [2](#)
- [39] Tero Karras, Miika Aittala, Jaakko Lehtinen, Janne Hellsten, Timo Aila, and Samuli Laine. Analyzing and improving the training dynamics of diffusion models. In *IEEE Conference on Computer Vision and Pattern Recognition (CVPR)*, 2024. [2](#)
- [40] Bahjat Kawar, Shiran Zada, Oran Lang, Omer Tov, Huiwen Chang, Tali Dekel, Inbar Mosseri, and Michal Irani. Imagic: Text-based real image editing with diffusion models. In *IEEE Conference on Computer Vision and Pattern Recognition (CVPR)*, 2023. [2](#)
- [41] kharchenkoirina. Fantasy fighting woman assassin actions in motion battle, hold daggers in hand. [See source](#). [18](#)
- [42] Yunji Kim, Jiyoung Lee, Jin-Hwa Kim, Jung-Woo Ha, and Jun-Yan Zhu. Dense text-to-image generation with attention modulation. In *IEEE International Conference on Computer Vision (ICCV)*, 2023. [3](#)
- [43] Alexander Kirillov, Eric Mintun, Nikhila Ravi, Hanzi Mao, Chloe Rolland, Laura Gustafson, Tete Xiao, Spencer Whitehead, Alexander C Berg, Wan-Yen Lo, et al. Segment anything. In *IEEE International Conference on Computer Vision (ICCV)*, 2023. [5](#), [8](#)
- [44] Vladimir Kolmogorov and Ramin Zabini. What energy functions can be minimized via graph cuts? *IEEE Transactions on Pattern Analysis and Machine Intelligence (TPAMI)*, 26(2), 2004. [3](#), [4](#)
- [45] Vivek Kwatra, Arno Schödl, Irfan Essa, Greg Turk, and Aaron Bobick. Graphcut textures: Image and video synthesis using graph cuts. *ACM Transactions on Graphics (TOG)*, 22(3), 2003. [3](#), [4](#)
- [46] Gabrielle Lamontagne. Snake. [See source](#), 2023. [18](#)
- [47] Yuseung Lee, Kunho Kim, Hyunjin Kim, and Minhyuk Sung. Syncdiffusion: Coherent montage via synchronized joint diffusions. In *Neural Information Processing Systems (NeurIPS)*, 2023. [3](#)
- [48] Yuheng Li, Haotian Liu, Qingyang Wu, Fangzhou Mu, Jianwei Yang, Jianfeng Gao, Chunyuan Li, and Yong Jae Lee. Gligen: Open-set grounded text-to-image generation. In *IEEE Conference on Computer Vision and Pattern Recognition (CVPR)*, 2023. [3](#)
- [49] Nan Liu, Shuang Li, Yilun Du, Antonio Torralba, and Joshua B Tenenbaum. Compositional visual generation with composable diffusion models. In *European Conference on Computer Vision (ECCV)*, 2022. [2](#)
- [50] Jian Ma, Junhao Liang, Chen Chen, and Haonan Lu. Subjectdiffusion: Open domain personalized text-to-image generation without test-time fine-tuning. In *ACM SIGGRAPH*, 2024. [3](#)
- [51] Chenlin Meng, Yutong He, Yang Song, Jiaming Song, Jiajun Wu, Jun-Yan Zhu, and Stefano Ermon. Sdedit: Guided image synthesis and editing with stochastic differential equations. In *International Conference on Learning Representations (ICLR)*, 2022. [2](#)
- [52] Chong Mou, Xintao Wang, Liangbin Xie, Yanze Wu, Jian Zhang, Zhongang Qi, and Ying Shan. T2i-adapter: Learning

- adapters to dig out more controllable ability for text-to-image diffusion models. In *Conference on Artificial Intelligence (AAAI)*, 2024. [2](#)
- [53] Alex Nichol, Prafulla Dhariwal, Aditya Ramesh, Pranav Shyam, Pamela Mishkin, Bob McGrew, Ilya Sutskever, and Mark Chen. Glide: Towards photorealistic image generation and editing with text-guided diffusion models. In *International Conference on Machine Learning (ICML)*, 2022. [2](#)
- [54] Maxime Oquab, Timothée Darcet, Théo Moutakanni, Huy Vo, Marc Szafraniec, Vasil Khalidov, Pierre Fernandez, Daniel Haziza, Francisco Massa, Alaaeldin El-Nouby, et al. Dinov2: Learning robust visual features without supervision. In *Transactions on Machine Learning Research (TMLR)*, 2023. [17](#), [22](#)
- [55] Gaurav Parmar, Krishna Kumar Singh, Richard Zhang, Yijun Li, Jingwan Lu, and Jun-Yan Zhu. Zero-shot image-to-image translation. In *ACM SIGGRAPH*, 2023. [2](#)
- [56] Gaurav Parmar, Taesung Park, Srinivasa Narasimhan, and Jun-Yan Zhu. One-step image translation with text-to-image models. *arXiv preprint arXiv:2403.12036*, 2024. [3](#)
- [57] Or Patashnik, Daniel Garibi, Idan Azuri, Hadar Averbuch-Elor, and Daniel Cohen-Or. Localizing object-level shape variations with text-to-image diffusion models. In *IEEE International Conference on Computer Vision (ICCV)*, 2023. [2](#)
- [58] William Peebles and Saining Xie. Scalable diffusion models with transformers. In *IEEE International Conference on Computer Vision (ICCV)*, 2023. [2](#)
- [59] Patrick Pérez, Michel Gangnet, and Andrew Blake. Poisson image editing. In *ACM SIGGRAPH*, 2003. [3](#), [4](#), [10](#)
- [60] Quynh Phung, Songwei Ge, and Jia-Bin Huang. Grounded text-to-image synthesis with attention refocusing. In *IEEE Conference on Computer Vision and Pattern Recognition (CVPR)*, 2024. [3](#)
- [61] Robin Rombach, Andreas Blattmann, Dominik Lorenz, Patrick Esser, and Björn Ommer. High-resolution image synthesis with latent diffusion models. In *IEEE Conference on Computer Vision and Pattern Recognition (CVPR)*, 2022. [1](#), [2](#)
- [62] Carsten Rother, Vladimir Kolmogorov, and Andrew Blake. “grabcut”: interactive foreground extraction using iterated graph cuts. *ACM Transactions on Graphics (TOG)*, 23(3), 2004. [3](#), [4](#)
- [63] Michael Rubinstein, Ariel Shamir, and Shai Avidan. Improved seam carving for video retargeting. *ACM Transactions on Graphics (TOG)*, 27(3), 2008. [3](#)
- [64] Vishnu Sarukkai, Linden Li, Arden Ma, Christopher Ré, and Kayvon Fatahalian. Collage diffusion. In *IEEE/CVF Winter Conference on Applications of Computer Vision (WACV)*, 2024. [3](#), [10](#), [16](#), [20](#)
- [65] Axel Sauer, Tero Karras, Samuli Laine, Andreas Geiger, and Timo Aila. Stylegan-t: Unlocking the power of gans for fast large-scale text-to-image synthesis. In *International Conference on Machine Learning (ICML)*, 2023. [2](#)
- [66] Axel Sauer, Dominik Lorenz, Andreas Blattmann, and Robin Rombach. Adversarial diffusion distillation. *arXiv preprint arXiv:2311.17042*, 2023. [2](#)
- [67] Takahiro Shirakawa and Seiichi Uchida. Noisecollage: A layout-aware text-to-image diffusion model based on noise cropping and merging. In *IEEE Conference on Computer Vision and Pattern Recognition (CVPR)*, 2024. [3](#)
- [68] Karen Simonyan and Andrew Zisserman. Very deep convolutional networks for large-scale image recognition. In *International Conference on Learning Representations (ICLR)*, 2015. [17](#), [22](#)
- [69] Werner Sobek. Heydar aliyev center. [See source](#). [18](#)
- [70] Jascha Sohl-Dickstein, Eric Weiss, Niru Maheswaranathan, and Surya Ganguli. Deep unsupervised learning using nonequilibrium thermodynamics. In *International Conference on Machine Learning (ICML)*, 2015. [2](#)
- [71] Yang Song, Jascha Sohl-Dickstein, Diederik P Kingma, Abhishek Kumar, Stefano Ermon, and Ben Poole. Score-based generative modeling through stochastic differential equations. In *International Conference on Learning Representations (ICLR)*, 2021. [2](#)
- [72] Yizhi Song, Zhifei Zhang, Zhe Lin, Scott Cohen, Brian Price, Jianming Zhang, Soo Ye Kim, and Daniel Aliaga. Object-stitch: Object compositing with diffusion model. In *IEEE Conference on Computer Vision and Pattern Recognition (CVPR)*, 2023. [3](#)
- [73] Richard Szeliski, Matthew Uyttendaele, and Drew Steedly. Fast poisson blending using multi-splines. In *IEEE International Conference on Computational Photography (ICCP)*, 2011. [3](#)
- [74] Ming Tao, Hao Tang, Songsong Wu, Nicu Sebe, Xiao-Yuan Jing, Fei Wu, and Bingkun Bao. Df-gan: Deep fusion generative adversarial networks for text-to-image synthesis. In *IEEE Conference on Computer Vision and Pattern Recognition (CVPR)*, 2022. [2](#)
- [75] Yoad Tewel, Omri Kaduri, Rinon Gal, Yoni Kasten, Lior Wolf, Gal Chechik, and Yuval Atzmon. Training-free consistent text-to-image generation. *ACM Transactions on Graphics (TOG)*, 43(4), 2024. [3](#)
- [76] Narek Tumanyan, Michal Geyer, Shai Bagon, and Tali Dekel. Plug-and-play diffusion features for text-driven image-to-image translation. In *IEEE Conference on Computer Vision and Pattern Recognition (CVPR)*, 2023. [2](#)
- [77] George Vogiatzis, Philip HS Torr, and Roberto Cipolla. Multi-view stereo via volumetric graph-cuts. In *IEEE Conference on Computer Vision and Pattern Recognition (CVPR)*, 2005. [4](#)
- [78] Wiii. Tōdai-ji kon-dō, at nara japan. [See source](#), 2008. [18](#)
- [79] Huikai Wu, Shuai Zheng, Junge Zhang, and Kaiqi Huang. Gp-gan: Towards realistic high-resolution image blending. In *ACM Multimedia (MM)*, 2019. [3](#), [10](#), [16](#), [21](#)
- [80] Binxin Yang, Shuyang Gu, Bo Zhang, Ting Zhang, Xuejin Chen, Xiaoyan Sun, Dong Chen, and Fang Wen. Paint by example: Exemplar-based image editing with diffusion models. In *IEEE Conference on Computer Vision and Pattern Recognition (CVPR)*, 2023. [2](#)
- [81] Hu Ye, Jun Zhang, Sibio Liu, Xiao Han, and Wei Yang. Ip-adapt: Text compatible image prompt adapter for text-to-image diffusion models. *arXiv preprint arXiv:2308.06721*, 2023. [2](#)

- [82] Jiahui Yu, Yuanzhong Xu, Jing Yu Koh, Thang Luong, Gungjan Baid, Zirui Wang, Vijay Vasudevan, Alexander Ku, Yinfei Yang, Burcu Karagol Ayan, et al. Scaling autoregressive models for content-rich text-to-image generation. In *International Conference on Machine Learning (ICML)*, 2022. [2](#)
- [83] Lingzhi Zhang, Tarmily Wen, and Jianbo Shi. Deep image blending. In *IEEE/CVF Winter Conference on Applications of Computer Vision (WACV)*, 2020. [3](#), [10](#), [16](#), [20](#)
- [84] Lvmin Zhang, Anyi Rao, and Maneesh Agrawala. Adding conditional control to text-to-image diffusion models. In *IEEE International Conference on Computer Vision (ICCV)*, 2023. [1](#), [2](#), [3](#), [4](#), [5](#), [18](#)
- [85] Richard Zhang, Phillip Isola, Alexei A Efros, Eli Shechtman, and Oliver Wang. The unreasonable effectiveness of deep features as a perceptual metric. In *IEEE Conference on Computer Vision and Pattern Recognition (CVPR)*, 2018. [10](#)
- [86] Yuxin Zhang, Weiming Dong, Fan Tang, Nisha Huang, Haibin Huang, Chongyang Ma, Tong-Yee Lee, Oliver Deussen, and Changsheng Xu. Prospect: Prompt spectrum for attribute-aware personalization of diffusion models. *ACM Transactions on Graphics (TOG)*, 42(6), 2023. [17](#), [23](#)
- [87] Shihao Zhao, Dongdong Chen, Yen-Chun Chen, Jianmin Bao, Shaozhe Hao, Lu Yuan, and Kwan-Yee K. Wong. Uni-controlnet: All-in-one control to text-to-image diffusion models. In *Neural Information Processing Systems (NeurIPS)*, 2023. [2](#)
- [88] Guangcong Zheng, Xianpan Zhou, Xuwei Li, Zhongang Qi, Ying Shan, and Xi Li. Layoutdiffusion: Controllable diffusion model for layout-to-image generation. In *IEEE Conference on Computer Vision and Pattern Recognition (CVPR)*, 2023. [3](#)
- [89] Minfeng Zhu, Pingbo Pan, Wei Chen, and Yi Yang. Dm-gan: Dynamic memory generative adversarial networks for text-to-image synthesis. In *IEEE Conference on Computer Vision and Pattern Recognition (CVPR)*, 2019. [2](#)

## A. Additional Results.

We include additional results in Figure 15 and 16. Figure 15 is an additional example of appearance mixing, where the user combines a green bird with blue wings and a yellow beak. Figure 16 is an additional example of improving prompt alignment. As shown, vanilla ControlNet struggles to correctly adhere to the long, complicated prompt. Using our method, the user can break the prompt up into multiple, short prompts and composite the images generated from the short prompts to form their desired image.

## B. Additional Baseline Comparisons

Here, we qualitatively compare our method with additional baselines, shown and summarized in Figure 17 and 18. Our method outperforms the baselines in terms of preserving local appearances and blending harmoniously. Below, we describe implementation details.

**CollageDiffusion [64].** We followed their released demo for generating baseline results. Their method allows users to tweak parameters per image layer and scene, such as added noise level and cross attention modulation, and then outputs a composite. We created the input image layers by resizing the masks from feature-space graph-cut to image space and applying them to each image. Reducing the added noise to zero preserves all local regions but with little harmonization (similar to copy-paste). To minimize changes, we used a set of parameters that preserves the background region (base image) but allows the foreground injected regions to change. We set noise levels to 0.05 for the base image and 0.4 for the non-base images. We set noise blur to 30 to smooth the seams. To ensure spatial fidelity of the image regions, we set the cross attention modulation of non-base images to 0.5, following their released examples. We also use their textual inversion feature and learn a special embedding for each image layer. If there are multiple image layers (regions) that correspond to the same word (e.g., multiple robot parts correspond to “robot” in the prompt “A robot from the future”), we choose the one that most closely matches the word description.

**Deep Image Blending [83].** We ran their released code to generate the baseline results. Their method takes in two images to composite (a source and target image) as well as a mask of the source image. To create the mask for each image, we resized the corresponding graph-cut mask from feature to image space. For composites of more than two input images, we iteratively ran Deep Image Blending on pairs of images to build towards the final composite. One input constraint is that their method takes square images as input, so we pre-process our image stack by resizing them to square images and resize the output back to the original aspect ratios.

**Blended Latent Diffusion + MultiDiffusion [4, 8].** We experimented with a modified version of Blended Latent Diffusion, where we fused the noises of different image regions with greater overlap, inspired by MultiDiffusion. Specifically, we dilate the mask of each region (in feature space) with a  $3 \times 3$  kernel and average the noise within the overlapped regions. As shown in Figure 17, this leads to artifacts near the seams (site of overlap) or changes local appearances.

**GP-GAN [79].** We ran their released code with their pre-trained model to generate the results. GP-GAN takes in two images to composite (a source and destination image), along with a mask of the source image to insert into the destination image. For composites of more than two images, we iteratively ran GP-GAN on pairs of images to build towards the final composite. We created the input masks by resizing the diffusion-space graph-cut results to the original resolution of each image.

**Cross-Domain Compositing [29].** Cross-Domain Compositing uses pre-trained Stable Diffusion models to compose images from different domains. We ran their released code and followed their examples for object immersion. Their method takes in a composite image and a foreground mask and outputs a harmonized image. Users can control the degree of local fidelity for foreground and background regions separately, at the expense of harmonization. Due to this trade-off, their method generally cannot preserve local appearances while also blending them together harmoniously. We created the input composite images by resizing the graph-cut masks from feature space to image space and compositing in image space. We treat the base image as the background, so the foreground mask covers regions from non-base images in the composite. To minimize changes, we applied the low-pass filter on the foreground region ( $N_{in} = 2, N_{out} = 1$ ). To reduce artifacts at the seams, we allowed the background region to change slightly in addition to the foreground region ( $T_{in} = 0.5, T_{out} = 0.9$ ).

**PCT-Net [28].** Given a composite image and a foreground mask, PCT-Net outputs a harmonized image by applying a spatially varying, per-pixel color transformation to the masked region. We ran their released code with their pre-trained model to generate the results. We created the input composite images by resizing the feature-space graph-cut masks into image space and compositing in pixel space. We treat the base image as the background, so the foreground mask covers regions from non-base images in the composite. To smooth seams between different regions, we dilated the foreground masks with a  $17 \times 17$  kernel to increase overlap.



## C. Additional Ablations

Here, we show additional ablation results on our graph cut and feature injection.

### C.1. Graph Cut

Our method uses the  $K$  features from self-attention layers to compute the graph cut energy terms, i.e., the pairwise terms which dictate seam costs. Here, we consider alternative features (Figure 19).

**$K$  features timesteps.** In our method, we use the  $K$  features from the last denoising step to set up the seam costs, when the image mostly formed. Here, we experiment with using earlier timesteps. Specifically, we experiment with  $K$  features averaged over: 1) the last half of denoising steps ( $t \geq 0.5$ ), and 2) all time steps ( $t \geq 0$ ). As shown in Figure 19, incorporating  $K$  features from earlier time steps lead to under-segmentations, where objects’ boundaries are not captured. This aligns with observations from previous works [14, 86] that earlier time steps form content and layout, while later time steps refine detailed appearance. By averaging earlier time steps, we weigh low-frequency content more heavily, thus leading to under-segmentations near boundaries.

**$Q$  and  $V$  features.**  $Q$  features lead to similar segmentations as  $K$  features but may exhibit over- and under-segmentations near boundaries (circled in Figure 19).  $V$  features generally do not lead to seams that align with semantic boundaries.

**VGG Features.** We experimented with VGG features [68] instead of diffusion features. Specifically, we extract the features from the second block’s ReLU layer, following Johnson et al. [36]. Figure 19 shows that VGG features typically leads to under-segmentations.

**DINOv2 Features.** We also experimented with DINOv2 features [54] in place of diffusion features. Specifically, we used the small DINOv2 model, which outputs features per  $14 \times 14$  patch. For fair comparison, we resized all images such that the size of output features would equal that of  $K$  features. As shown in Figure 19, if we directly apply our graph cut method (which uses the features’ top-10 PCA components), we see errors in segmentation. If we use the top-100 PCA components, we get better segmentations for most examples but not all (e.g., the dog in Figure 19d).

**Discussion.** While we chose to go with  $K$  features due to the best segmentation, we found that our feature blending method is robust to small errors in segmentation boundaries. For example, the segmentations we get from  $Q$  features are similar to that of  $K$  features. While  $Q$  features may result in over- or under-segmentations near boundaries, our feature blending method blends the seams well, such that the difference in the resulting images is not too noticeable

(Figure 20).

### C.2. Feature Injection

Our method injects the composite  $Q^{\text{comp}}, K^{\text{comp}}, V^{\text{comp}}$  into the U-Net’s self-attention maps for all layers and time steps. Following related works in self-attention injection [2, 14], we consider injecting only in decoder layers and in later time steps.

**Layers.** ControlNet with Stable Diffusion v1.5 has three decoder blocks (D1, D2, D3). We experimented with injecting in subsets of these blocks (D1-D3, D2-D3, D3). In many cases, injecting only the decoder layers (D1-D3) lead to similar results as our method (which injects all layers). However, in some cases, it may lead to artifacts and structural changes (e.g., waffle texture in Figure 21a), and it often reduces color vibrancy and saturation (e.g., bird feathers in Figure 21b) in the composite output.

**Time Steps.** We used a total of 20 denoising time steps for all our results. Prior work shows that earlier denoising time steps form image layout and shape, while later time steps form detailed appearance [14, 86]. We experimented with applying our injection after 5, 10, and 15 time steps. As shown in Figure 22, starting the injection later tends to create artifacts in the blended output. In most cases, starting the injection after 5 time steps lead to comparable results to our method (which injects all time steps). However, in scenes that require the image structure to adapt near the seams, doing so may prevent the model from adapting sufficiently. For example, if we inject after 5 time steps, the shadow from the removed rock at the apple bite still shows up in the final image (circled in red), whereas it is completely removed if we apply the injection for all time steps.

**Discussion.** If the required adaption near seams is minor, and the user does not mind changes to local appearances, one can consider applying the injection only in decoder layers (D1-D3) and after 5 time steps. This will require less storage space for the initially generated  $Q, K, V$  feature vectors, as only the features in the relevant layers and time steps will need to be stored. However, if the user wishes to maximize adaptation near seams and to maximize local appearance fidelity, we recommend using our full injection approach.

## D. User Survey Details

We launched two anonymous user surveys among computer science graduate students, in order to compare our method with three other baselines (Interactive Digital Photomontage [1], Blended Latent Diffusion [4], MasaCtrl+ControlNet [14]). For each of the 12 scenes (Figures 5, 6, 7, 15), we created results using our method and the three baselines. For each scene, we showed the four results side-by-side and asked users to select the best result. The order of the



Figure 14. **User Survey (Blending)**. We show users the input images and selected regions to blend, and then ask them pick the best result from four images: one generated by our method, and the others generated by Digital Photomontage, Blended Latent Diffusion, and MasaCtrl+ControlNet.

four images are randomized for each scene, and the order of scenes are also randomized in each survey.

In the first survey, we asked “Which of the following images appear most realistic to you?” In the second survey, we showed the input images and asked users to pick the image that is the best at blending them. Specifically, we showed the full input images as well as the graph-cut regions (to be blended) on each input image. To help users focus on the individual image regions, we darken out other parts of the input image (Figure 14). Then, we asked “Which of the following images are BEST at blending all the selected image regions shown on top?”

Users are asked to complete the first survey (realism) before the second survey (blending) to avoid bias. We received 16 completed surveys for the realism one (total of 192 responses across all scenes) and 10 completed surveys for the blending one (total of 120 responses across all scenes).

## E. Result Details

We used various Stable Diffusion pre-trained models (v1.5) to generate results in this paper. Specifically, we used the canny edge model (Figures 5d, 6a,d,e, 7, 15), the scribble model (Figures 5b,c,e, 6b), the depth map model (Figure 5a), the Openpose model (Figure 6c), and the HED model

(Figures 13, 16).

The input conditions (e.g., edge map, sketches) are manually created or derived from images released by ControlNet [84] or found on the web [3, 19, 41, 46, 69, 78].

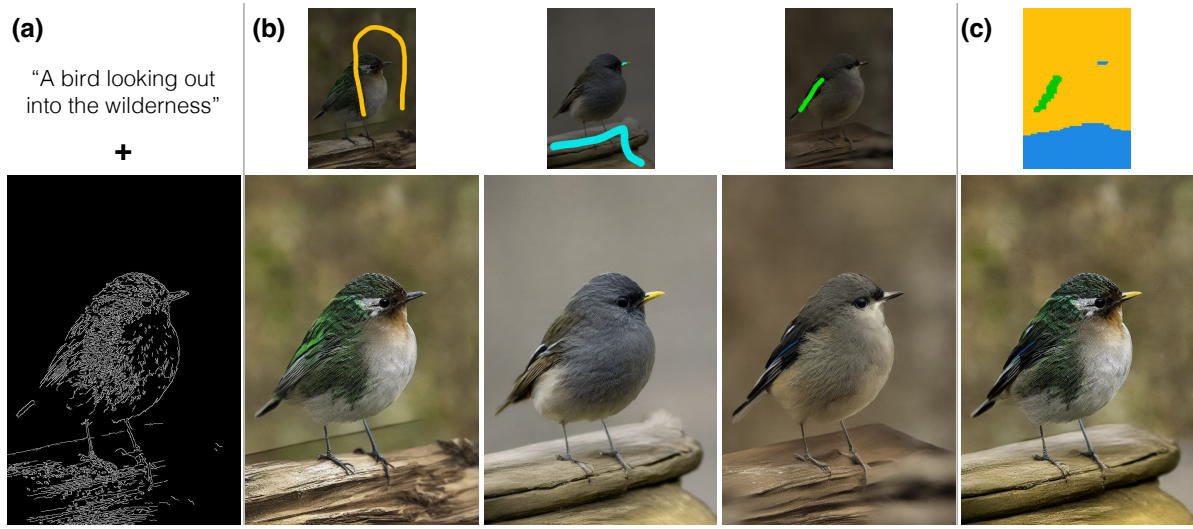


Figure 15. **Additional Result: Bird.** Users can combine feather colors of birds. (a) Input to vanilla ControlNet. (b) The user selects the green feathers in the first image, the yellow beak and foothold of the second image, and the blue wings from the third image. (c) Generative Photomontage’s graph cut (top) and final output (bottom).



Figure 16. **Additional Result: Little Red Riding Hood.** (a) Vanilla ControlNet struggles to adhere to the long, complicated prompt, i.e., it assigns the wrong color to scene elements. (b) The user can instead generate a stack of images with multiple, short prompts, where each spatial region has at least one correct image within the stack. User strokes are shown on top of each image. (c) Generative Photomontage composites the user-selected regions together (bottom), where each scene element has the correct color according to the original, long prompt. Top: feature-space graph-cut result.

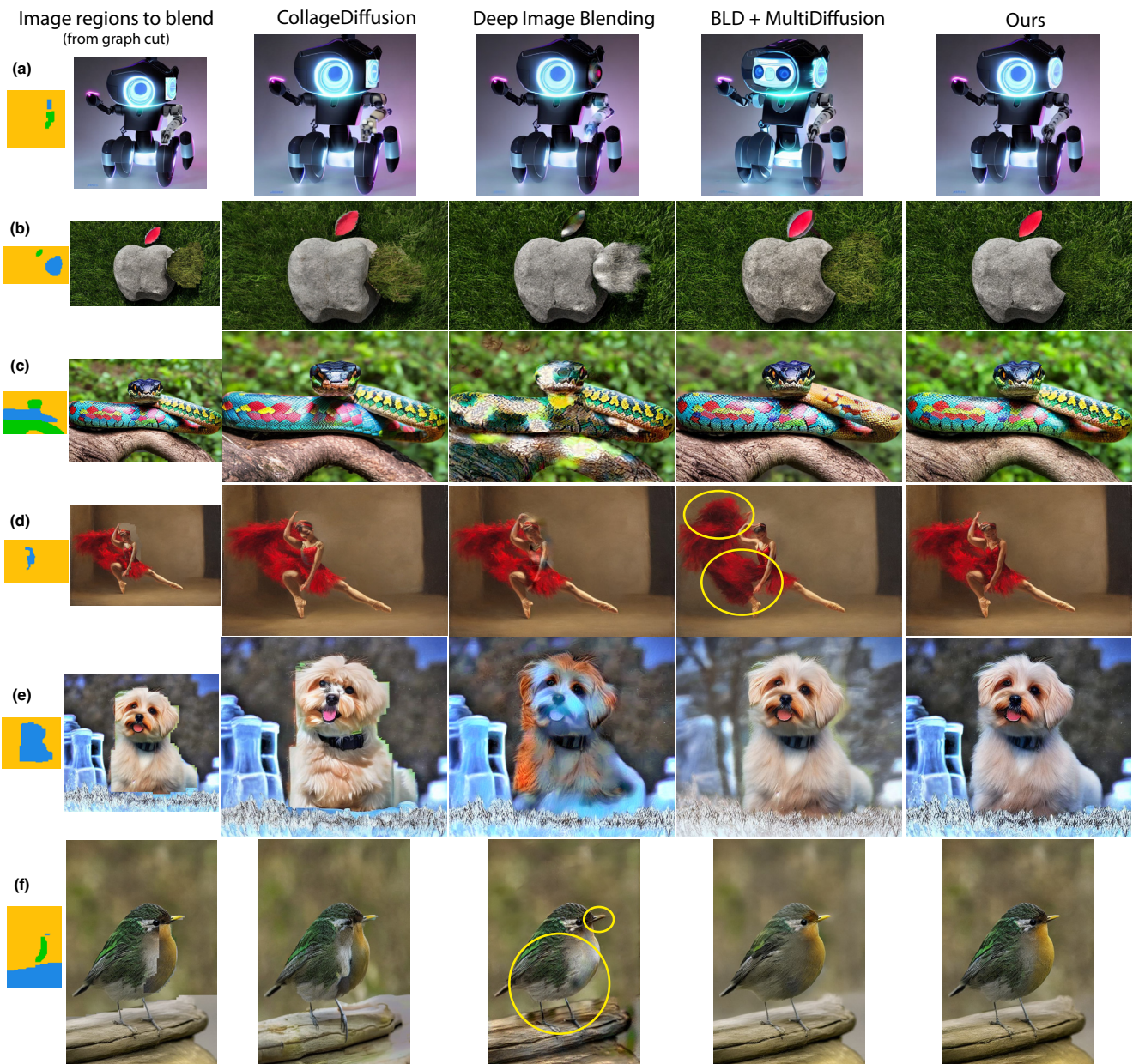


Figure 17. **Qualitative Comparison (Additional Baselines)**. Leftmost column: Image regions to blend (output of graph-cut optimization). Graph-cut in diffusion feature space is visualized on the left, and the image-space composite of that graph-cut is visualized on the right. CollageDiffusion [64] may struggle to preserve local appearance (b, c, d) or blend regions harmoniously (a, b, e, f). Deep Image Blending [83] may also fail to preserve local appearances (a) or show artifacts in the blended regions (b-f). Blended Latent Diffusion + MultiDiffusion [4, 8] may show artifacts at the seams, where the noise of overlapping regions are blended together (b, e), or fail to preserve local appearances (a, c, d, f).

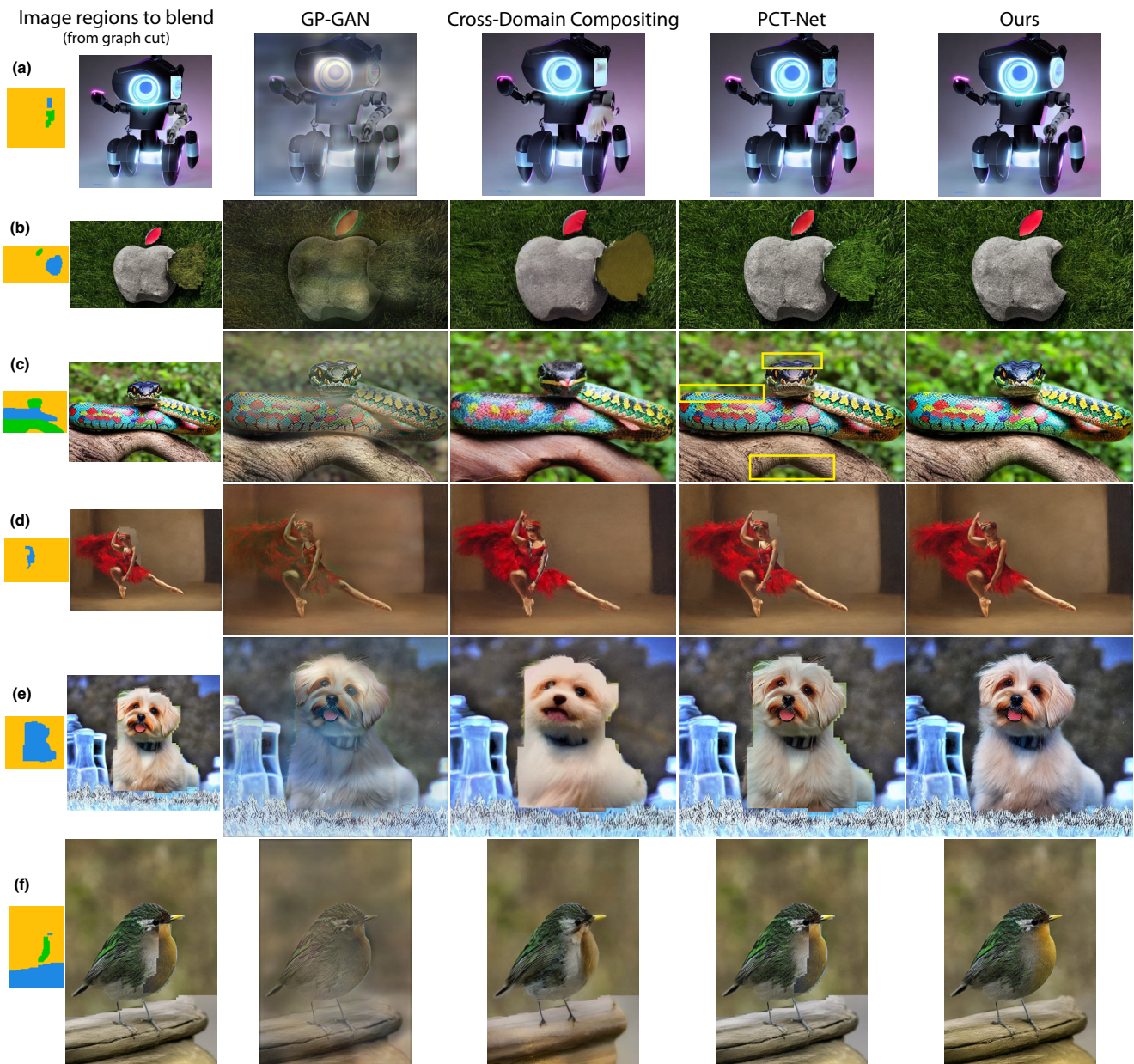


Figure 18. **Qualitative Comparison (Additional Baselines)**. Leftmost column: Image regions to blend (output of graph-cut optimization). Graph-cut in diffusion feature space is visualized on the left, and the image-space composite of that graph-cut is visualized on the right. GP-GAN [79] does not preserve local appearances and tends to smooth out color. Cross-Domain Compositing [29] may struggle to blend regions harmoniously, particularly in non-oil painting style images (a-c, e-f). PCT-Net [28] changes the interior color of local regions but struggles to blend away the seams.



Figure 19. **Ablation: Graph Cut Features.** Our method uses the self-attention  $K$  features to compute pairwise seam costs in the optimization. Here, we experiment with using the  $K$  features averaged across different time steps, the other self-attention features  $Q$  and  $V$ , as well as VGG [68] and DINOv2 [54] features.  $K$  features performs the best, with  $Q$  features a close second.

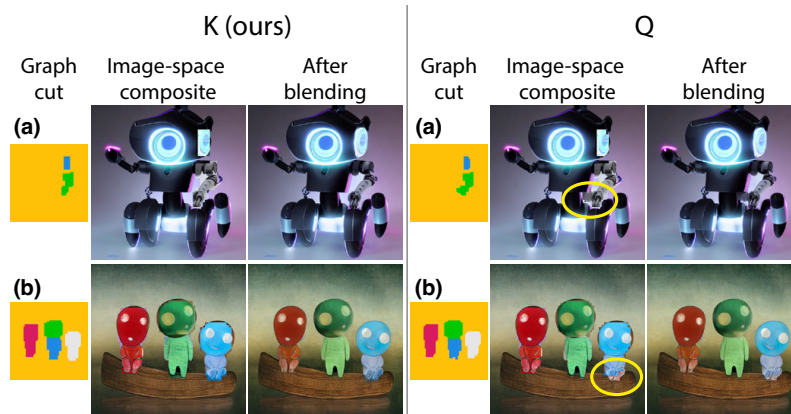


Figure 20. **Effects of Segmentation on Feature Blending.** Our feature blending method is robust to small errors in segmentation boundaries. For example, while  $Q$  features may result in over- or under-segmentations near boundaries, our feature blending method blends the seams well, such that the difference in the resulting images is not too noticeable.

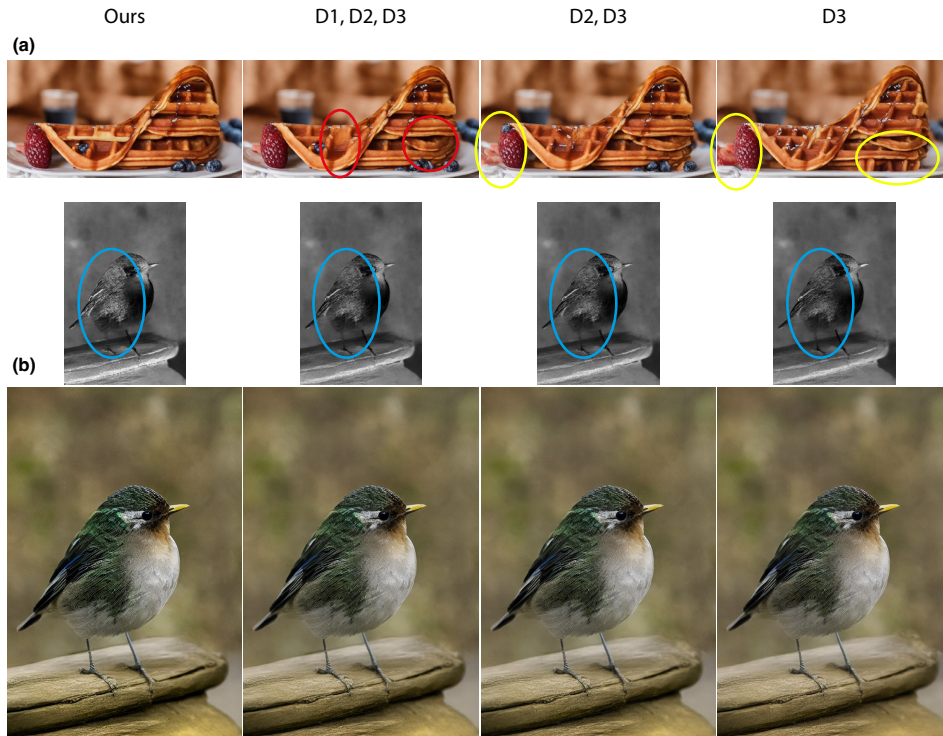


Figure 21. **Ablation: Injection Layers.** Experiments of injecting  $Q^{\text{comp}}, K^{\text{comp}}, V^{\text{comp}}$  only in decoder blocks (D1, D2, D3) of ControlNet. (a) Injecting only in the decoder blocks leads to changes in the waffle interior (circled in red). As we reduce the number of injected layers, more artifacts and local changes appear, such as the extra strawberry and missing blueberries (circled in yellow). (b) Injecting only in the decoder layers also tends to reduce color vibrancy in the composite image. Saturation is visualized above each image (white: high saturation; black: low saturation). As shown, the color saturation of bird feathers is reduced in the ablated results (circled in blue).

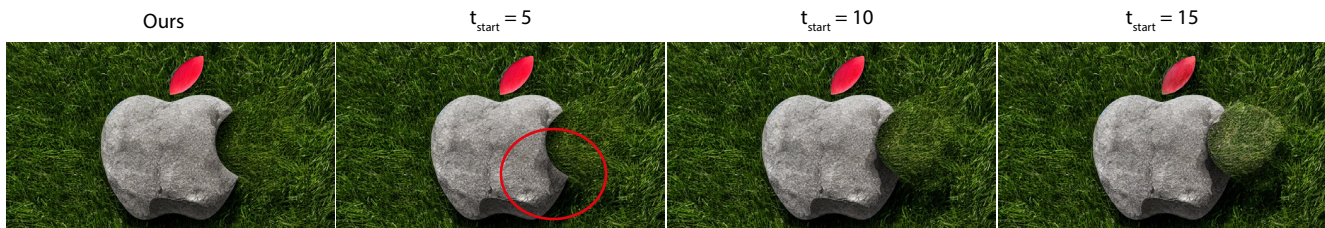


Figure 22. **Ablation: Injection Time Steps.** Experiments of injecting  $Q^{\text{comp}}, K^{\text{comp}}, V^{\text{comp}}$  after a number of time steps ( $t_{\text{start}}$ ) during the denoising process (total: 20 time steps). As shown, starting the injection later leads to more artifacts. Our results ( $t_{\text{start}} = 0$ ) completely removes the extra rock at the apple bite and also removes the shadow of the extra rock. However, when  $t_{\text{start}} = 5$ , we see the shadow still remains on the base rock. This aligns with previous observations that earlier time steps form image layout and shape [14, 86], so starting the injection process later reduces the model’s ability to adapt image structure near the seams.